



Trade Science Inc.

ISSN : 0974 - 7486

Volume 9 Issue 5

Materials Science

An Indian Journal

Full Paper

MSAIJ, 9(5), 2013 [168-175]

Responses to indentation and to impedance spectroscopy of plastically compressed steels. Part 1: Case of pure iron

Adrien Frigerio¹, Pierre-Yves Girardin¹, Patrice Berthod^{2*}

¹Lycée Henri Loritz, 29 Rue des Jardiniers 54000 Nancy, (FRANCE)

²Institut Jean Lamour (UMR CNRS 7198), Department CP2S, Team “Surface and Interface, Chemical Reactivity of Materials”, University of Lorraine, B.P. 70239, 54506 Vandoeuvre-les-Nancy, (FRANCE)

E-mail: patrice.berthod@univ-lorraine.fr

ABSTRACT

The consequences of plastic deformation of alloys on their electrochemical behaviour may be usefully known to anticipate changes in corrosion resistance. Stationary methods of corrosion characterization can be helped by transitory methods to complete the knowledge about the hardening – corrosion dependence. Impedance spectroscopy was used in this work to study the effect of several compression plastic deformations on the corrosion behaviour of a model metallic material – pure iron – for the two main orientations of surface with respect to the deformation axis. It appeared here that the electrochemical behaviour of crystalline iron after plastic deformation immersed in an acid sulphuric aqueous solution can be still described by the same electro-kinetic model as usually considered for the not-deformed iron, independently from the deformation rate and from the orientation of the surface versus the compression axis. In addition it varies with these two but not really monotonously, except for two of the three studied deformation rates. Indeed, in this case it appeared for example that the charge transfert resistance tends to be higher for the parallel orientation than for the perpendicular one and increases for both orientations with the deformation rate.

© 2012 Trade Science Inc. - INDIA

KEYWORDS

Pure iron;
Compression;
Plastic deformation;
Hardness;
Corrosion;
Impedance spectroscopy.

INTRODUCTION

In many metallurgical fabrication processes metals and alloys are subjected to plastic deformation to obtain the required shapes for the pieces. This induces changes in the defects states of the microstructures (notably concerning the dislocation densities) and then changes in the material properties, the mechanical ones as well as the surface reactivity. If, on the one hand, the effect of plastic deformation on the mechanical

behaviour can be generally described by a hardening of the alloys, the reported observations concerning the corrosion behaviour are much more scattered. For a given alloy this can be attributed to several possible causes: difference of deformation mode, difference of deformation amount, or difference of surface orientation versus the direction of the initial deformation. In order to try uncoupling these possible factors a first study^[1] was initiated for pure iron and ternary austenitic stainless steel by elaborating by foundry cylinders,

by plastically deforming cylindrical parts in compression at different rates, by cutting samples to obtain electrodes with either a surface parallel to the deformation axis or perpendicular to this axis, and by performing electrochemical tests consisting in linear or cyclic polarizations to assess the corrosion characteristics in the active state as well as in the passive state using the Stern-Geary and Tafel methods for instance.

The aim of the present work is to complete the previous observations by estimating the effects of the direction and rates of deformation, on the alloy hardness and by further characterizing the electrochemical behaviours of the electrodes made of the deformed alloys with the determination of the transfert resistance and the double layer capacitance by using impedance spectroscopy, a well-known experimental method used for corrosion characterization^[2] which was for example recently used for steels^[3-7] as well as for other metals or alloys (Cr and Zn deposits^[8], copper^[9], aluminium^[10], bronzes^[11] ...).

EXPERIMENTAL

Elaboration of the as-cast iron cylinders and compression runs

Small parts of pure iron (purity of more than 99.9 wt.%, total of about 40g) were melted together using the High Frequency induction technique in inert atmosphere (CELES furnace, 300mbars of pure Argon). The aspiration in a silica tube dived in the levitating liquid allowed its solidification as a about four centimetres long full cylinder with a diameter of about 10 mm. The obtained cylindrical ingot was thereafter cut in several cylindrical parts which were, except one, subjected to a more or less intense compression in order to obtain several permanent deformation rates with compression runs performed with a MTS-RF/150 testing machine. The three compression curves corresponding to the three targeted deformation rates (-12.5%, -25% and -40%) are displayed superposed in Figure 1 while the photographs presented in Figure 2 show the cylindric samples before and after compression. Their initial and final dimensions are given in TABLE 1 and the yield stresses measured on the curves are given in TABLE 2.

TABLE 1 : Values of the diameters and heights of the sample before and after compression test (without stress applied, measured using a numeric caliper); deformation rates really obtained.

IRON	Low compression	Medium compression	High compression
initial diameter (mm)	10.71	10.68	10.70
initial height (mm)	8.51	11.75	10.41
final height (mm)	7.68	9.17	6.87
deformation (%)	-9.75	-22.2	-34.0

TABLE 2 : Values of the yield strength in compression.

IRON	Low compression	Medium Compression	High compression
Yield strength Re (MPa)	31	69	67

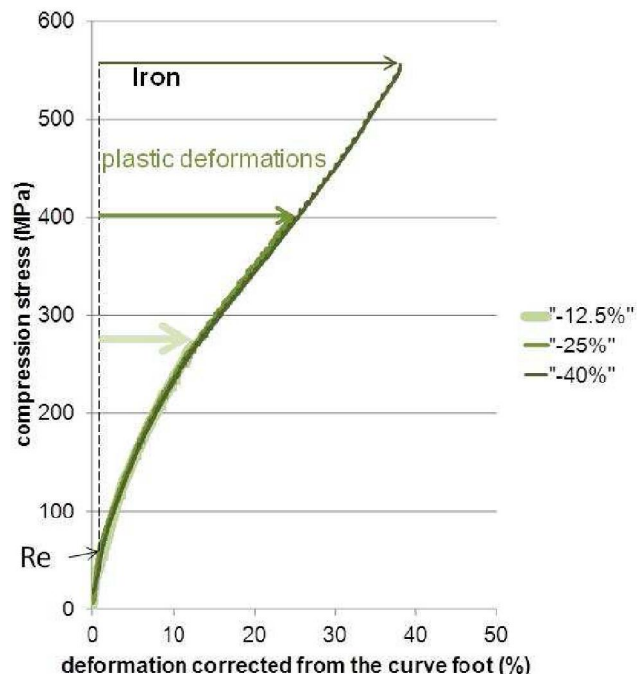


Figure 1 : Superposition of the three compression curves.

As-cast	Deformed		
		-9.75%	(obtained, against -12.5% targeted)
		-22.2%	(obtained, against -25% targeted)
		-34.0%	(obtained, against -40% targeted)

Figure 2 : The three samples destined to compression (initial and final states).

Preparation of the metallographic samples and of the electrodes

The as-cast sample and the three deformed samples were cut using a precision saw (Isomet 5000 of Buelher),

Full Paper

following a procedure already presented^[1] and which can be graphically resumed by Figure 3. This procedure allows obtaining a metallographic sample (respectively an electrode) showing (resp. exposing to the electrolyte) a surface which is either parallel or perpendicular to the deformation axis (which is also the cylinder axis).

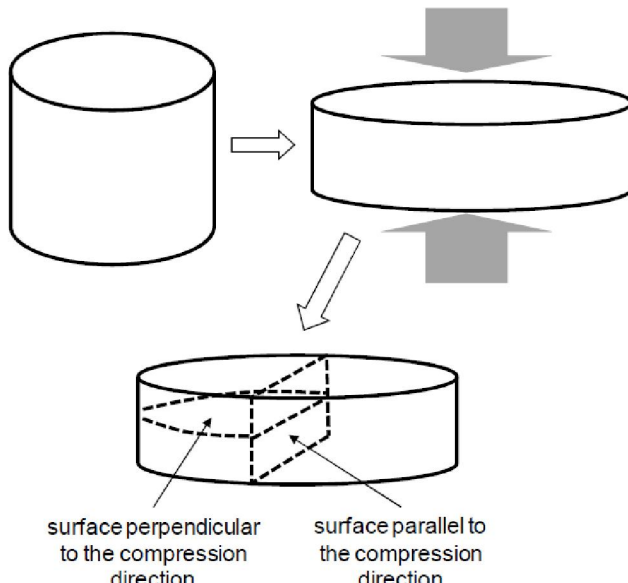


Figure 3 : Cutting procedure for obtaining a surface parallel to the compression axis and a surface perpendicular to the compression axis.

In each case the part for metallography and the part for electrode were embedded in a cold resin (ESCL: Araldite CY230 and hardener HY 956) mixture (after having been connected to a plastic-covered copper electrical wire in the case of the electrode). The metallographic sample and the electrode surfaces were thereafter polished with SiC papers up to 1200-grit (and ultrasonically cleaned then polished to mirror-state with 1 µm-particles pastes for the metallographic sample).

Metallographic observations and Vickers indentations

The metallographic samples were observed after Nital etching (ethanol + 4% HNO₃, immersed during about ten seconds, then water-washed to stop attack and dried). This allowed thereafter controlling the nature and the deformed states of the microstructure using an Olympus optical microscope. Runs of X-Ray Diffraction were additionally performed using a Philips X'Pert Pro diffractometer (wavelength Cu Kα) to control the crystalline network of the as-cast and the de-

formed samples. Vickers indentations were performed using a Testwell Wolpert machine with a load of 10kg. Three indentations were realized for each {deformation rate × surface orientation} combination, with subsequently calculation of the average and standard deviation values.

Impedance spectroscopy runs

The EIS runs were performed in a sulphuric acid aqueous solution, H₂SO₄ 2N, using a {three electrodes}-cell composed of the working electrode (the studied sample), a Saturated Calomel Electrode (SCE) for the reference in potential, and a graphite rod for the counter electrode. The potentiostat which was used is an Ametek one driven by the Versastudio software. After the determination of the Open Circuit Potential the applied E varied alternatively between E_{ocp}-10mV and E_{ocp}+10mV with a frequency decreasing from 100,000Hz down to 1Hz. This was repeated five times: at t=1 minute after immersion, t= 6 min, t= 11 min, t= 16 min and t= 21 min.

RESULTS AND DISCUSSION

Microstructure characterization

Metallographic samples are all ferritic, as seen after Nital etching and microscope observation, and as confirmed by the obtained XRD spectra. These ones, displayed in Figure 4 for the parallel orientation and in Figure 5 for the perpendicular orientation, effectively present the main diffraction peaks (110, 211 and 200 for the not too high angles) of bcc iron^[12]. It seems that the plastic deformation in compression tends to reduce the peaks in the case of the parallel orientation while, on the contrary, it tends to enhance them for the perpendicular orientation. Indeed the peaks for the {-34%}-deformed state are especially small in the parallel case and the ones for the same deformation rate are particularly high in the perpendicular case.

Vickers indentations

The evolution of the hardness with the deformation rate is illustrated by the two superposed curves presented in Figure 6, one corresponding to the parallel orientation and the other corresponding to the perpendicular orientation. One can see that the hardness logi-

cally increases with the deformation rate (typically +100Hv points for 34% of deformation in compression) with seemingly a tendency to slightly higher values for the perpendicular orientation by comparison with the parallel orientation.

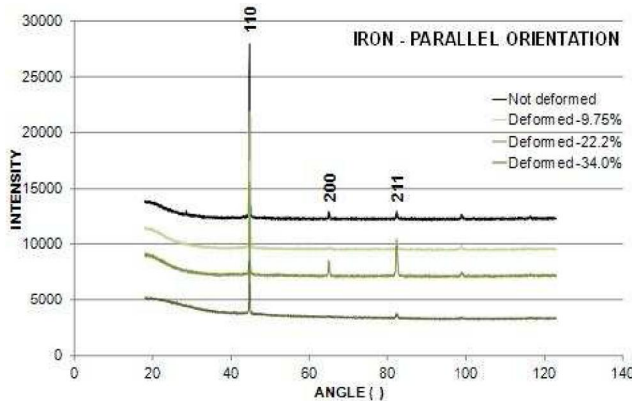


Figure 4 : XRD patterns obtained for the not-deformed state and for the three deformed states (parallel orientation).

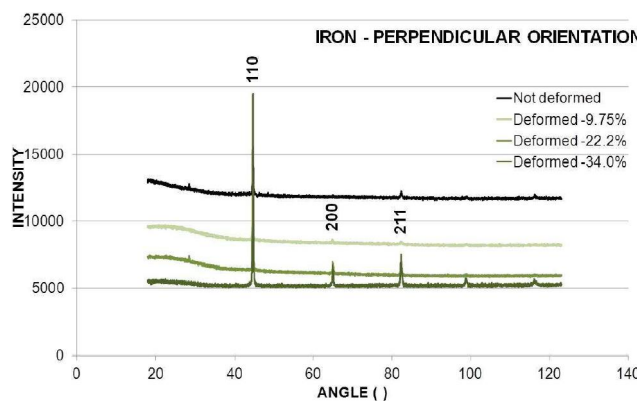


Figure 5 : XRD patterns obtained for the not-deformed state and for the three deformed states (perpendicular orientation).

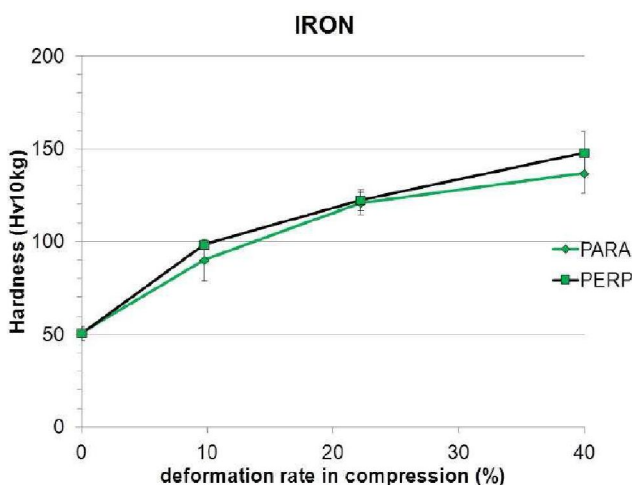


Figure 6 : Evolution of the Vickers hardness versus the deformation rate and for the two orientations.

Impedance spectroscopy

The EIS results are displayed as Nyquist diagram $\{Z_{\text{imag}} = f(Z_{\text{real}})\}$ in Figure 7 for the not-deformed state and the perpendicular orientation only (problems occurred during the EIS run for the parallel orientation) and in Figure 8 for all the deformed states and the two orientations. This shows that all these Nyquist diagrams are similar to half a circle (however the radius along the Z_{imag} axis tends to be lower than the one along the Z_{real} axis). One can see on Figure 7 (which also reminds the exploitation of such Nyquist diagram when this one is close to half a circle) that the circle diameter tends to slightly decrease with time. The inverse evolution seems occurring for the {-9.75%}- and {-34.0%}-deformed states for the two orientations while the evolution is not monotonous for the intermediate {-22.2%}-deformed state.

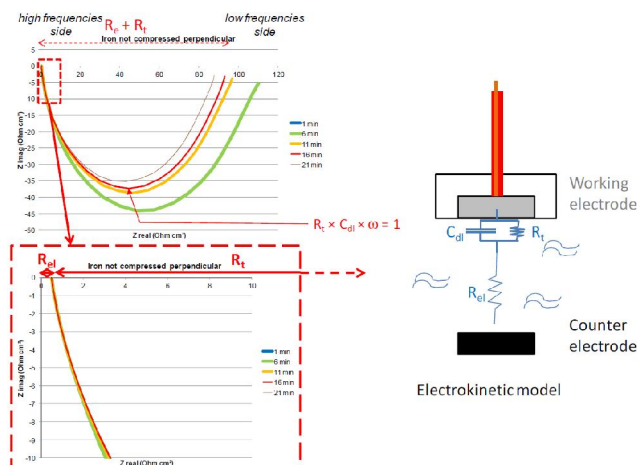


Figure 7 : Nyquist plot of the EIS results for the not-deformed sample and the perpendicular orientation.

Concerning the effect of orientation on the circle size one can see in Figure 9, Figure 10 and Figure 11, where the Nyquist diagram at all times and for the two orientations are superposed for each deformation rate value, that the diameter tends to be slightly higher for the parallel orientation than for the perpendicular one for -9.75% of deformation, inversely significantly lower for the parallel orientation than for the perpendicular one for -22.2%, and higher again for the parallel orientation than for the perpendicular orientation for -34% of plastic deformation.

The EIS results were more quantitatively exploited, according to the few reminders given in Figure 7, to extract, of the one hand the values of the electrolyte

Full Paper

resistance and of the charge transfert resistance (the sum of which is the polarization resistance: $R_p = R_{el} +$

R_t), and of the other hand the values of the capacitance of the Gouy-Chapman double layer.

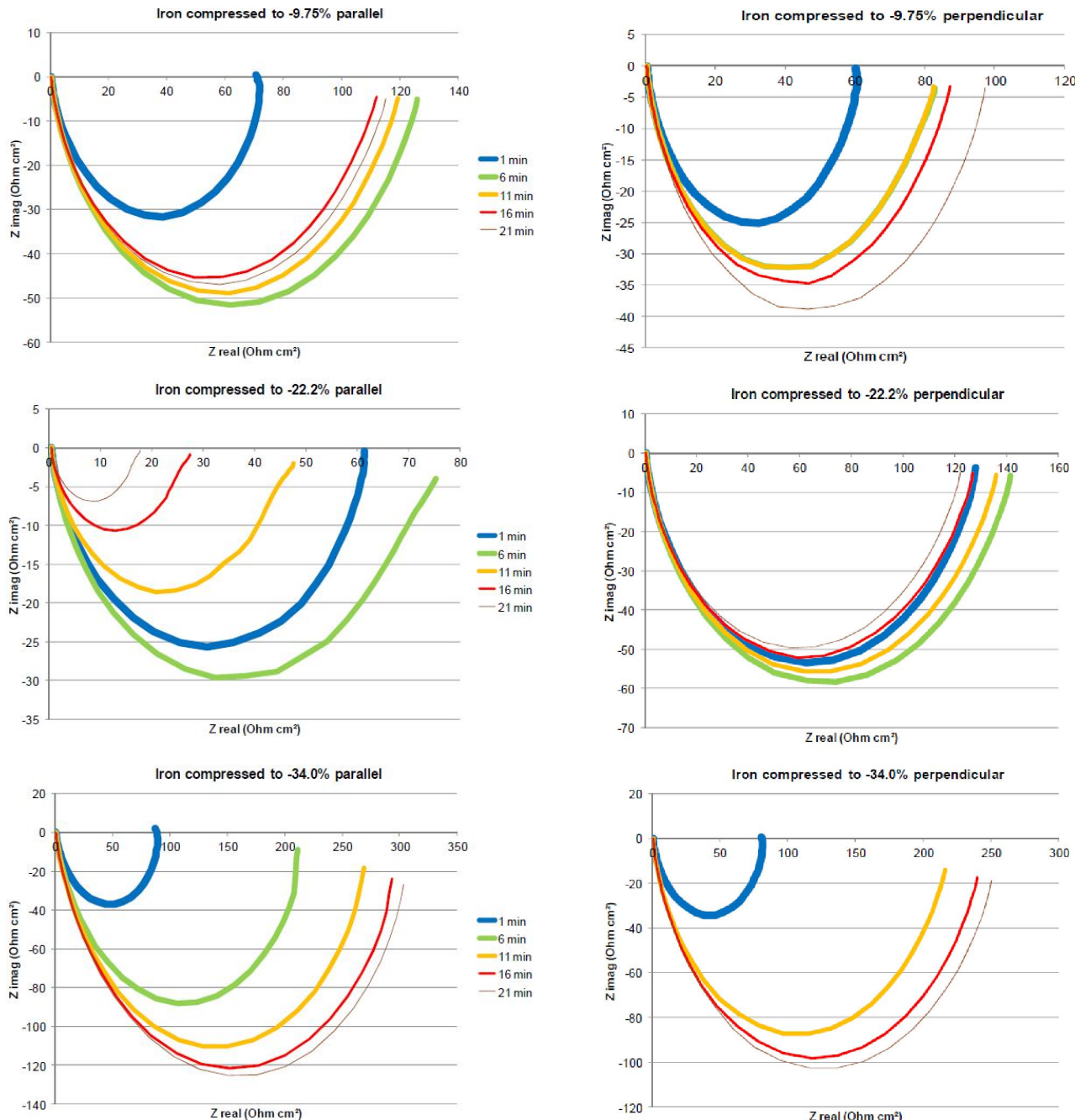


Figure 8 : Nyquist plot of the EIS results for the three deformation states (top: -9.75%, middle: -22.2%, bottom: -34.0%) and the two orientations (left: parallel, right: perpendicular).

Logically the electrolyte resistance (automatically identified as being the smallest abscissa value) did not vary with time during each experiment (TABLE 3). Indeed the distance between the working electrode and the counter electrode was constant. Its value was low, of about 0.4-0.5 Ohm cm² in much cases, but of 0.65

Ohm cm² in one case (-34.0% perpendicular). Knowing the electrolyte resistances in all cases, the determination of the charge transfert resistance from the maximal abscissa (the R_{el} value being then deduced) was more accurate. The values obtained for R_t , listed in TABLE 4, are generally at the { 100 Ohm cm²} - level

with, at all time, a difference between the parallel orientation and the perpendicular orientation for a given deformation rate. The mismatch at all times is in the same direction between the two orientations for the -9.75% deformation state and for the -34.0% deformation state (transfert resistance slightly higher for the parallel orientation than for the perpendicular orientation) while the inverse difference can be seen for the -22.2% deformation state (with in addition a mismatch increasing with time).

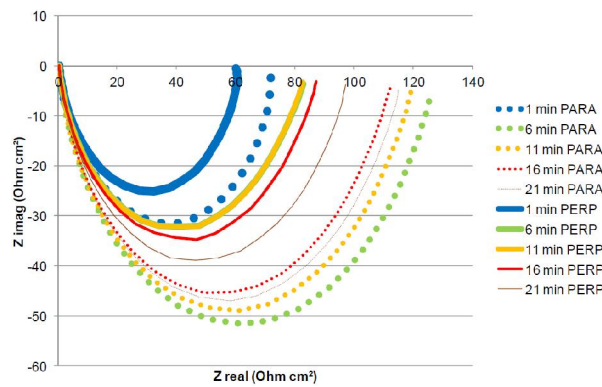


Figure 9 : Superposition of the Nyquist diagrams parallel and perpendicular for the -9.75% deformation state.

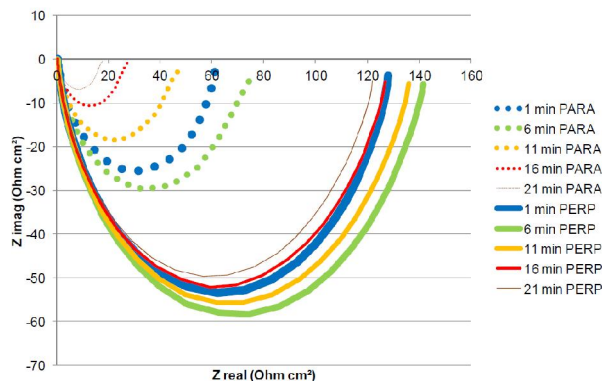


Figure 10: Superposition of the Nyquist diagrams parallel and perpendicular for the -22.2% deformation state.

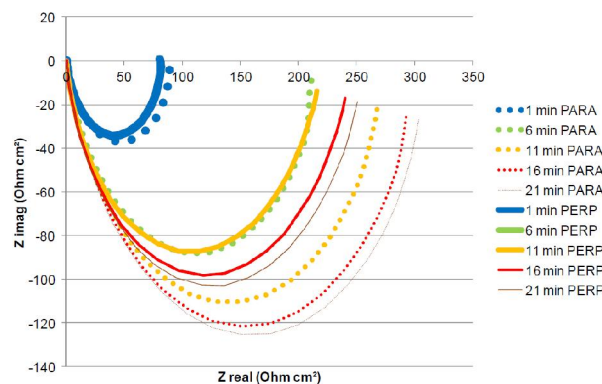


Figure 11: Superposition of the Nyquist diagrams parallel and perpendicular for the -34.0% deformation state.

TABLE 3 : Value of the electrolyte resistance versus the deformation rate and the orientation.

R _{el} (Ohm cm ²)	Orientation	t=1 min	t=6 min	t=11 min	t=16 min	t=21 min
Not deformed	PARA	/	/	/	/	/
	PERP	/	0.497	0.495	0.495	0.494
	-9.75%	PARA	0.414	0.419	0.420	0.421
		PERP	0.417	0.423	0.427	0.428
	-22.2%	PARA	0.491	0.502	0.506	0.507
		PERP	0.456	0.459	0.459	0.458
	-34.0%	PARA	0.445	0.450	0.449	0.450
		PERP	0.653	/	0.660	0.660

TABLE 4 : Value of the transfer resistance versus the deformation rate and the orientation.

R _t (Ohm cm ²)	orientation	t=1 min	t=6 min	t=11 min	t=16 min	t=21 min
Not deformed	PARA	/	/	/	/	/
	PERP	/	109.6	96.4	92.7	87.4
	-9.75%	PARA	71.5	125.6	119.0	111.8
		PERP	60.3	82.4	82.2	86.8
	-22.2%	PARA	61.0	74.8	47.1	27.0
		PERP	127.6	141.1	135.5	126.4
	-34.0%	PARA	88.6	211.1	268.5	293.1
		PERP	81.0	/	215.7	239.7

The summit of the circle, which was reached for a frequency decreasing when the deformation rate increases (TABLE 5) at least for the perpendicular orientation, allowed determining the double layer capacitance, knowing now the charge transfer resistance. The calculated values are rather variable but remain close to about $0.2\text{--}0.3 \times 10^{-3}$ Farad / cm² and no well established dependence on the deformation rate and on the orientation can be revealed.

TABLE 5 : Value of the frequency corresponding to the Nyquist circle summit versus the deformation rate and the orientation.

f circle summit(Hz)	orientation	t=1 min	t=6 min	t=11 min	t=16 min	t=21 min
Not deformed	PARA	/	/	/	/	/
	PERP	/	63.1	63.1	63.1	79.4
	-9.75%	PARA	63.1	39.8	39.8	39.8
		PERP	63.1	50.1	50.1	39.8
	-22.2%	PARA	79.4	79.4	125.9	199.5
		PERP	39.8	31.6	31.6	39.8
	-34.0%	PARA	39.8	20.0	12.6	12.6
		PERP	63.1	/	20.0	20.0

Full Paper

TABLE 6 : Value of the double layer capacitance versus the deformation rate and the orientation.

	C _{dl} .10 ⁻³ F/cm ²	Orientation	t=1 min	t=6 min	t=11 min	t=16 min	t=21 min
Not deformed		PARA	/	/	/	/	/
		PERP	/	0.145	0.165	0.171	0.144
-9.75%		PARA	0.222	0.200	0.211	0.225	0.219
		PERP	0.263	0.242	0.243	0.289	0.259
-22.2%		PARA	0.207	0.168	0.168	0.186	0.183
		PERP	0.197	0.224	0.233	0.199	0.207
-34.0%		PARA	0.283	0.237	0.296	0.271	0.262
		PERP	0.196	/	0.232	0.209	0.200

The values of open circuit potential just before each of the EIS experiments were also noted and they are presented in TABLE 7. These values show that all the samples were in the active state, this confirming the rather low values of R_t and then of R_p.

TABLE 7 : Evolution of the open circuit potential versus time for the different deformation rates and for the two orientations.

	E _{ocp} (/NHE, mV)	orientation	t=1 min	t=6 min	t=11 min	t=16 min	t=21 min
Not deformed		PARA	/	/	/	/	/
		PERP	-265	-265	-256	-252	-251
-9.75%		PARA	-255	-271	-265	-259	-257
		PERP	-274	-281	-275	-272	-271
-22.2%		PARA	-262	-267	-252	-237	-226
		PERP	-270	-271	-267	-263	-261
-34.0%		PARA	-248	-267	-268	-269	-268
		PERP	-263	/	-279	-278	-277

General commentaries

The compression of these iron samples was easy to do thanks to their cylindrical shapes allowed by the foundry procedure which was chosen (aspiration of the molten metal in a silica tube). The mechanical deformation first showed the maximal elastic stresses which were conform to what is usually measured for not-alloyed ferritic steels (less than 100 MPa) and rather high deformations were possible to obtain (up to 34% of relative deformation in compression) thanks to the high capacity of the testing machine. This allowed achieving hardened states for these samples for which Vickers indentation tests lead to significantly higher values of hardness by comparison with the ones obtained for the as-cast condition, a classical effect which was also re-

cently observed for a ferrite-pearlitic steel^[13]. However no significant difference of hardness was observed between the two orientations, differently to what was seen for the ferrite-pearlitic steel mentioned above^[13]. Concerning the electrochemical tests one saw that for all the deformation states and for the two orientations the Nyquist plots led to semicircles (more precisely half of ellipsoids). The exploitation of these Nyquist diagrams was attempted according to the electrochemical model reminded in Figure 7. Unfortunately, despite some evolutions which can be noted, no well established general dependence – valid for the three deformation states – was really seen. Nevertheless, if one removes the -22.2%-deformation state from the presented results, it may appear in TABLE 4 that the charge transfer resistance, which tends to be higher for the parallel orientation than for the perpendicular orientation at all immersion times, increases with the compression rate, here too for all times of immersion. In addition the frequency corresponding to the circle summit appears to be at all times lower for the parallel orientation than for the perpendicular one and it decreases in the two cases if the plastic deformation in compression increases. In contrast, always the results obtained for -22.2% considered as removed, the double layer capacitance should not show clear variation.

CONCLUSIONS

Despite the rather high deformation rates achieved on crystalline iron in this study, and then the resulting strong hardening levels which notably resulted in significantly increased hardness for the most compressed samples, the corrosion behaviour of the more or less deformed samples did not show clear evolution. However it appeared that impedance spectroscopy may reveal some interesting effects of the plastic deformation, as well as of the orientation of the studied surface with respect to the deformation axis, on some characteristics only reachable by using EIS runs, as the charge transfer resistance. Unfortunately the medium deformation rate tested here did not allow highlighting such effect which then needs to be further studied – and maybe confirmed – by an additional work. Notwithstanding these first results show that the effect of a preliminary hardening on the corrosion behaviour can be deeper

investigated by the transitory methods to enrich the first observations done by the stationary ones.

REFERENCES

- [1] P.Y.Girardin, A.Frigerio, P.Berthod; Materials Science: An Indian Journal, **9(4)**, 123 (2013).
- [2] D.Landolt; Traité des matériaux-N°12 Corrosion et chimie de surface des métaux, Presses Polytechniques et Universitaires Romandes, Lausanne, (1997).
- [3] M.Sanchez, H.Mahmoud, M.C.Alonso; Journal of Solid State Electrochemistry, **16(3)**, 1193 (2012).
- [4] J.J.Shi, W.Sun; Fushi Kexue Yu Fanghu Jishu, **23(5)**, 387 (2011).
- [5] X.Li, Y.Wang, C.Du, B.Yan; Journal of Nanoscience and Nanotechnology, **10(11)**, 7226 (2010).
- [6] A.Hemmasian-Ettefagh, M.Amiri, C.Dehghanian; Materials Performance, **49(3)**, 60 (2010).
- [7] Y.Ma, Y.Li, F.Wang; Corrosion Science, **51(5)**, 997 (2009).
- [8] M.M.T.Luque, J.J.O.Florez, H.Del Lujan; Ingenieria y Desarrollo, **29(2)**, 170 (2011).
- [9] B.Rosborg, T.Kosec, A.Kranjc, J.Pan, A.Legat; Electrochimica Acta, **56(23)**, 7862 (2011).
- [10] J.Ma, J.Wen, X.Lu, Y.Li; Fushi Yu Fanghu, **30(6)**, 373 (2009).
- [11] D.Satovic, L.V.Zulij, V.Desnica, S.Fazinic, S.Martinez; Corrosion Science, **51(8)**, 1596 (2009).
- [12] E.P.Elsukov, V.M.Fomin, D.A.Vytovtov, G.A.Dorofeev, A.V.Zogainov, N.B.Arsenteva, S.F.Lomaeva; Phys.Met.Metallogr., **100**, 251 (2005).
- [13] E.Conrath, P.Berthod; Materials Science: An Indian Journal, **9(3)**, 107 (2013).